APL Materials

RESEARCH ARTICLE | OCTOBER 24 2024

Incommensurate superlattice modulation surviving down to an atomic scale in sputter-deposited Co/Pt(111) epitaxial multilayered films

Jieyuan Song ; Thomas Scheike ; Cong He ; Zhenchao Wen ; Tadakatsu Ohkubo ; Kwangseok Kim; Hiroaki Sukegawa ; Seiji Mitani

APL Mater. 12, 101120 (2024)
https://doi.org/10.1063/5.0233911
CHORUS

Incommensurate superlattice modulation surviving down to an atomic scale in sputter-deposited Co/Pt(111) epitaxial multilayered films

Cite as: APL Mater. 12, 101120 (2024); doi: 10.1063/5.0233911
Submitted: 18 August 2024 • Accepted: 10 October 2024 •
Published Online: 24 October 2024

Jieyuan Song,[1,2,a] Thomas Scheike,[1] Cong He,[1] Zhenchao Wen,[1] Tadakatsu Ohkubo,[1] Kwangseok Kim,[3] Hiroaki Sukegawa,[1,a] and Seiji Mitani[1,2]

AFFILIATIONS

[1] National Institute for Materials Science (NIMS), Tsukuba 305-0047, Japan
[2] Graduate School of Science and Technology, University of Tsukuba, Tsukuba 305-8577, Japan
[3] Samsung Advanced Institute of Technology, Suwon-si 16678, South Korea

[a] **Authors to whom correspondence should be addressed:** song.jieyuan@nims.go.jp and sukegawa.hiroaki@nims.go.jp

ABSTRACT

We report the structural feature of sputter-deposited epitaxial [Co (0.2 nm)/Pt (0.2–1.0 nm)] multilayered films prepared with various periodic structural designs consisting of non-integer numbers of Co and Pt monoatomic layers on an atomically flat Ru(0001). Sharp superlattice modulation peaks and their systematic changes with the Pt thicknesses were observed in the x-ray diffraction (XRD) spectrum. The formation of periodic structures shows that layer-by-layer like growth occurs and the resulting incommensurate superlattice modulation survives down to an atomic scale even in the sputter-deposited Co/Pt multilayers. Magnetic properties were also investigated for the Co/Pt multilayers. Interestingly, the maximum perpendicular magnetic anisotropy K_u of 3×10^6 erg/cm^3 was obtained for the [Co (0.2 nm)/Pt (0.3 nm)] multilayer exhibiting incommensurate superlattice modulation peaks, while the [Co (0.2 nm)/Pt (0.2 nm)] multilayer with a $L1_1$-like XRD peak showed a smaller K_u. A cross-sectional high-angle annular dark-field scanning transmission electron microscopy analysis revealed that a partially $L1_1$-ordered CoPt structure is formed in the [Co 0.2 nm/Pt 0.2 nm] multilayer, interpreting the observed K_u. This study gives a new insight into the structural feature of sputter-deposited Co/Pt multilayers useful for a wide range of spintronic devices, such as magnetic tunnel junctions.

In recent years, there has been a noteworthy memory revolution toward the stimulating cutting-edge technologies such as machine learning, artificial intelligence, and neuromorphic applications. Magnetoresistive random access memory (MRAM) is one of the outstanding candidates for next-generation random access memory technology, and Co/Pt multilayered films with strong perpendicular magnetic anisotropy (PMA) are known as an indispensable building block for MRAMs.[1–4] More recently, a novel magnetic tunnel junction (MTJ) structure with an $L1_1$-CoPt ordered alloy corresponding to the Co/Pt(111) monoatomic multilayer in the structure has also been predicted theoretically with tunnel magnetoresistance (TMR) ratios over 2000% due to an interfacial resonant tunneling effect.[5] Furthermore, the $L1_1$-CoPt ordered alloy may be considered for a potential PMA material for future recording media. A merit from an application point of view is that the Co/Pt multilayers exhibit a large magnetocrystalline anisotropy energy density (K_u) along with a relatively low-temperature treatment around 300 °C, especially for forming the $L1_1$ metastable phase.[1,6]

Although molecular beam epitaxy (MBE) techniques were historically used to fabricate high-quality metallic multilayers,

sputtering is a low-cost and efficient way, especially for manufacturing. Sato *et al.* reported a high K_u of 37 × 10^6 erg/cm^3 for CoPt alloy films deposited by a co-sputter method.[1] Yakushiji *et al.* developed a superlattice structure of sputter-deposited Co/Pt multilayers, as well as their sharp interface.[6] The layer-by-layer stacking and fcc(111) ordered-alloy-like structure were revealed for the Co/Pt multilayers by a microstructure analysis. However, the growth mechanism of Co/Pt multilayers still remains unclear, and such studies encourage us to investigate the Co/Pt superlattice structure in light of both artificial superlattices and naturally formed $L1_1$-ordered alloys. Compared with the co-sputter method, it is likely that atomic-scale multilayer sputter-deposition enables us to form superlattices with improved controllability and stability.

In this article, epitaxial Co/Pt multilayer structures were fabricated by magnetron sputtering with various Pt concentrations at a low pressure of 0.3 Pa. The well-optimized growth conditions maintained a high flatness and crystallinity. The superlattice/crystal structure, magnetic properties, and microstructure are discussed. A peak splitting of the $L1_1$ superlattice feature was observed by the out-of-plane x-ray diffraction (XRD) spectrum, which indicates the well-controlled non-integer monoatomic layer growth, i.e., incommensurate superlattice formation. This is a surprising result, because such a superlattice consisting of non-integer numbers of monoatomic layers has only been reported by the MBE method so far.[7,8] The Pt content dependence of magnetic properties, including the saturation magnetization (M_s) and the anisotropy field (H_k), and K_u, is also summarized. The microstructure analysis revealed the formation of a partially $L1_1$ ordered-like structure existing inside the Co/Pt multilayers.

All stacks were deposited by magnetron sputtering (EIKO Corporation) on a single crystal sapphire Al_2O_3(0001) substrate at a base pressure below 9 × 10^{-7} Pa. A high-quality 40 nm Ru buffer was deposited on a thermal-cleaned substrate. Then, the Co/Pt multilayer was deposited by alternate sputtering of non-integer monoatomic controlled Co and Pt thin layers. A series of samples with substrate/Ru 40 nm/[Co 0.2 nm/Pt x nm]$_y$ multilayer/Ru 2 nm cap stack were deposited, and the total thickness of the [Co/Pt] layer was fixed around 10 nm for consistency. Here, one monolayer (ML) for Co and Pt is calculated as 0.21 and 0.23 nm, respectively. The Co layer thickness is fixed at ~1 ML, and the Pt layer thickness x varies from 0.2 to 1.0 nm, which corresponds to 1–5 ML of Pt. y is the repetition number of Co/Pt bilayers. Before the deposition, the sapphire substrates were baked in the muffle furnace (AS ONE HPN-ON) at 1000 °C for 1 h with an air atmosphere for better surface flatness. In the vacuum chamber, the substrates were first degassed at 860 °C for 1 h, and then, the Ru buffer was deposited 30 min later after stopping the heating and the monitored temperature was around 345 °C. *In situ* post-annealing was carried out at 850 °C for 1 h for the optimization of the surface flatness and crystallinity. The Co/Pt multilayer was also deposited 1 h later after stopping the heating of the Ru post-annealing process, and the monitored temperature was around 293 °C. This strategy aimed at maintaining a stable environment since the substrate heating may induce temperature fluctuation varied with the output power. The deposition of Ru and Co/Pt was performed at an Ar ambience of 0.1 and 0.3 Pa, since the low-pressure deposition may yield a better growth quality for both the roughness and crystallinity. The sputtering power for each target is direct current (DC) 40 W for Ru, radio frequency (RF) 40 W for Co, and RF 40 W for Pt. The deposition rate for each layer is Ru 0.061 nm/s, Co 0.014 nm/s, and Pt 0.011 nm/s.

All samples were characterized by atomic force microscopy (AFM) for surface morphology analysis. The crystal structures were characterized by *in situ* reflection high energy electron diffraction (RHEED) and *ex situ* XRD with Cu $K\alpha$ radiation (wavelength: 0.154 18 nm) and a graphite monochromator. The magnetic properties were analyzed using a vibrating sample magnetometer (VSM), and the perpendicular anisotropy energy $K_u = H_k M_s/2$ was estimated from the M_s and H_k from the in-plane and out-of-plane magnetization–magnetic field (M–H) loops at room temperature. The microstructure analysis was identified by the high-resolution high-angle annular dark-field scanning transmission electron microscopy (HAADF-STEM) and the energy dispersive x-ray spectroscopy (EDS) (FEI Titan G2 80-200 ChemiSTEM).

We first investigated the structural properties as shown in Fig. 1. Figure 1(b) shows the 5 × 5 μm^2 area AFM image with a very flat surface morphology of an Al_2O_3(0001) substrate/Ru (40 nm)/[Co 0.2 nm/Pt 0.2 nm]$_{24}$/Ru 2 nm stack. The average roughness R_a = 0.15 nm and the peak-to-valley value P–V = 2.35 nm are listed on the graph. The well-established flatness can be attributed to the high-temperature *ex situ* baking for substrate and *in situ* post-annealing for the Ru buffer layer. The RHEED pattern of this stack is shown in Figs. 1(c)–1(f) with an incident electron beam along the $Al_2O_3[10\bar{1}0]$ azimuth for (c) Co/Pt and (d) Ru buffer and along the

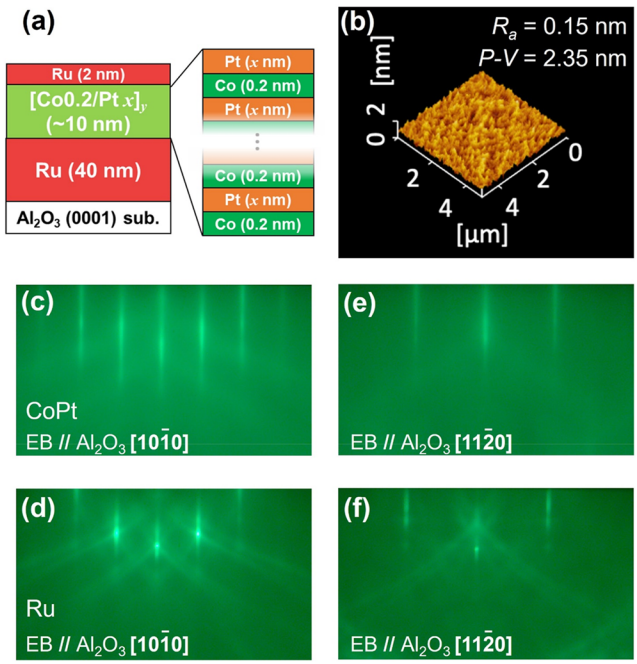

FIG. 1. (a) Illustration of a Ru buffer (40 nm)/[Co 0.2 nm/Pt 0.2 nm]$_{24}$/Ru 2 nm stack. (b) AFM image of the sample surface. RHEED patterns of (c) and (e) Co/Pt and (d) and (f) Ru buffer surfaces. The incident electron beam is parallel to (c) and (d) $Al_2O_3[10\bar{1}0]$ and (e) and (f) $Al_2O_3[11\bar{2}0]$ azimuths.

$Al_2O_3[11\bar{2}0]$ azimuth for (e) Co/Pt and (f) Ru buffer. The observation was performed after the post-annealing process of the Ru layer. The patterns taken from the Ru(0001) surface have distinct Kikuchi lines, indicating that a highly crystallized and oriented Ru buffer was achieved due to the well-optimized deposition profile. In the next step, an epitaxial Co/Pt multilayer was deposited with the RHEED patterns shown in Fig. 1. The 30° rotation from an $Al_2O_3[10\bar{1}0]$ to $Al_2O_3[11\bar{2}0]$ azimuth proved the sixfold symmetry with respect to the perpendicular axis. Suppose that the Co/Pt layer has a fcc-like structure as a fundamental lattice, the epitaxial relationship between Ru(0002) and CoPt(111) can be defined as $Al_2O_3(0001)[11\bar{2}0]$ || $Ru(0001)[10\bar{1}0]$ || $CoPt(111)[11\bar{2}]$. Since it is difficult to distinguish fundamental fcc and $L1_1$ ordered structures only by RHEED results,[9] further analysis of the crystal structure should be conducted with the XRD and STEM measurements. Note that all samples with Co/Pt multilayers and various Pt thicknesses showed similar RHEED patterns in the surface flatness and epitaxial growth.

Figure 2 shows the out-of-plane XRD results for the Co/Pt multilayers with various nominal Pt thicknesses of 0.2, 0.3, 0.4, 0.5, 0.6, and 1.0 nm. The stacking structure was kept as substrate/Ru 40 nm/[Co 0.2 nm/Pt x nm]$_y$ multilayer/Ru 2 nm cap, in which only the Pt layer thickness x and the repetition numbers (y) changed, making the total thickness of the Co/Pt multilayer nearly constant [around 10 nm; see Fig. 2(a)]. The epitaxial growth of the Ru buffer layer with the high-intensity Ru (0002) peak and (0004) peak alongside the substrate peaks was observed for the XRD results of all the samples shown in Fig. 2(b). For the [Co 0.2 nm/Pt 0.2 nm]$_{24}$ sample, a sharp superlattice peak associated with the $L1_1$ ordered structure can be observed at 20.5° and the corresponding d-spacing is 0.43 nm, which is consistent with the [Co 1 ML/Pt 1 ML] structure. The relatively low intensity of the $L1_1$-CoPt peak indicates that the compositional contrast between Co (rich) and Pt (rich) monoatomic layers is incomplete in this configuration of structural design. There are no peaks other than the CoPt(111)-oriented peaks so that the full epitaxial growth of Ru and fcc(111)-like Co/Pt layers is confirmed by the XRD.

With increasing the Pt layer thickness, each multilayer period of the Co/Pt samples increased systematically. A distinctive peak-splitting behavior was observed as shown in Fig. 2. In previous reports,[7,8] the peak positions of superlattice reflections can be given by

$$q_s = \frac{2\pi n}{\bar{d}} \pm \frac{2\pi m}{\Lambda}, \tag{1}$$

where the integer n represents the index of the main reflection peaks, the integer m means the index of the mth satellite peak, $\bar{d}$ is the average lattice spacing, and Λ is the modulation wavelength of the superlattice. Λ can be treated as the total thickness of one period and written as $\Lambda = N\bar{d}$, in which N stands for the total number of lattice planes in one period. Here, N can be not only integer (commensurate superlattice) but also non-integer (incommensurate superlattice). For the Co/Pt(111) superlattice structure consisting of alternate stacks of Co(111) and Pt(111) monolayers, $\bar{d}$ represents the mean value of individual thickness of each layer. Hereafter, we define that $n = 0$ and $n = 1$ correspond to the fundamental (000) and (111) peaks, respectively. The $\pm m$th satellite peak associated with the fundamental peak will be designated as $0^{\pm m}$ and $1^{\pm m}$. For instance, the Co/Pt multilayer with a period of [Co 0.2 nm (~1 ML)/Pt 0.2 nm

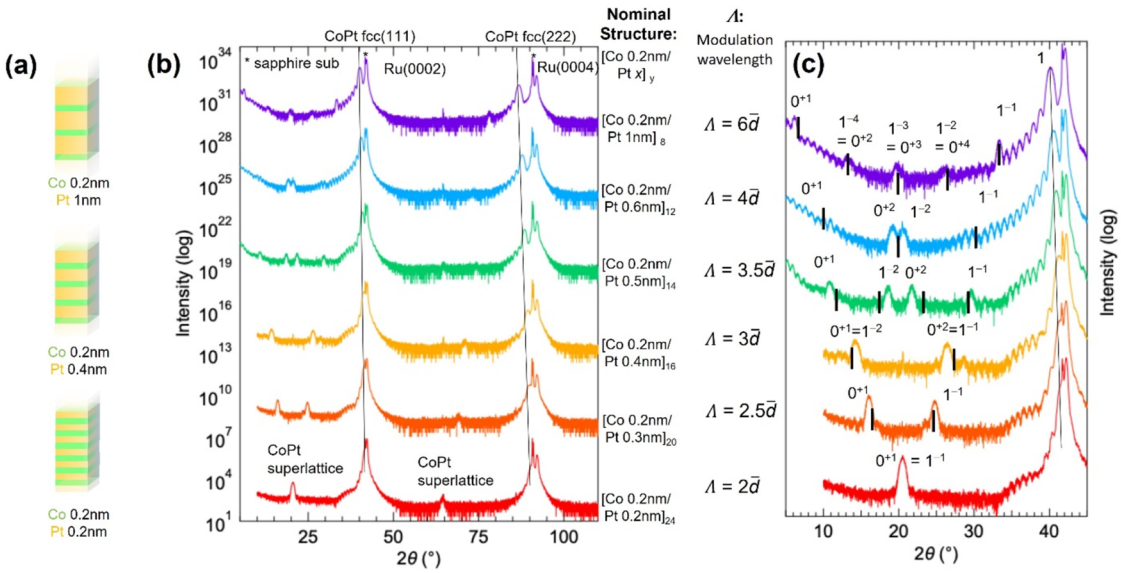

FIG. 2. (a) Illustration of nominal structures for Co/Pt multilayers. (b) XRD profiles for the substrate/Ru 40 nm/[Co 0.2 nm/Pt x nm]$_y$ multilayers/Ru 2 nm sample series. The exact structure of Co/Pt multilayers and the superlattice modulation wavelengths Λ are listed. (c) A focused region of peak splitting depicted from (b). The labels $n^{\pm m}$ represent the mth satellite peaks of the nth fundamental fcc reflections [$n = 0$ represents fcc(000); $n = 1$ represents fcc(111)]. The | marks are the calculated peak positions based on the effective d-spacing $d_{(n^{\pm m})}$ from Eq. (2) and Bragg's law.

(~1 ML)] has N = ~2 and Λ = ~2$\bar{d}$ so that the position of the 0^{+1} peak and 1^{-1} peak can coincide with each other, if a commensurate Co/Pt superlattice is formed. In fact, the observed 0^{+1} and 1^{-1} peaks result in a single superlattice peak at 2θ = 20.5°, as shown in the bottom and red color spectrum of Fig. 2(b). With increasing the Pt thickness, N increases and the positions of 0^{+1} and 1^{-1} peaks start to differ from each other, resulting in separate peaks and constructing the peak splitting feature as shown in a series of the XRD spectra. In the high angle region, the higher Co/Pt superlattice peak around 60° also splits, although the intensity of the satellite peaks is rather low.

Figure 2(c) shows a focused region of the low-angle peak splitting behavior taken from Fig. 2(b). To identify the effective lattice spacing $d_{(n^{\pm m})}$ for a satellite peak $n^{\pm m}$, we can assume that the allowed peak position $q_{(n^{\pm m})} = \frac{2\pi}{d_{(n^{\pm m})}}$. From Eq. (1), it can also be written as $q_{(n^{\pm m})} = \frac{2\pi n}{\bar{d}} \pm \frac{2\pi m}{N\bar{d}}$; then, we can deduce

$$d_{(n^{\pm m})} = \frac{N}{nN \pm m}\bar{d}. \quad (2)$$

When n = 1 and m = 0 [the fundamental (111) peak labeled by "1" in Fig. 2(c)], we can evaluate the average lattice spacing $\bar{d}$ from the peak position of the fundamental (111) experimentally. For N equal to 2.5, 3, 3.5, 4, and 6, the $\bar{d}$ values were evaluated as 0.218, 0.219, 0.220, 0.223, and 0.225 nm, respectively. Namely, with increasing the Pt thickness, the fundamental (111) peak is gradually shifted, as distinguished by the solid line. Note that for the 1.0 nm Pt sample, the (111) and (222) peak positions are almost the same as the bulk Pt(111) and Pt(222).

The 2θ value for each satellite peak can be calculated with Eq. (2) and Bragg's law, and the results were marked with " | " on the XRD spectra in Fig. 2(c). The mark positions agree with the experimental results. As for $\Lambda = 3\bar{d}$, $3.5\bar{d}$, and $4\bar{d}$, the deviation may be caused by errors of the total thickness. If we use $2.8\bar{d}$, $3.73\bar{d}$, and $4.2\bar{d}$, the differences between calculations and experiments are less than 0.4°. This indicates that the accuracy of the present thickness control in the sputter deposition is within ~0.2 ML.

Such an intentionally introduced incommensurate superlattice structure, which can be indexed quantitatively with m, n, and non-integer N through the relationship between the fundamental and satellite peaks, was only reported for MBE-grown multilayer samples.[7,8] Surprisingly, even for the non-integer N values by "sputter deposition," the peak splitting is still well-defined in the

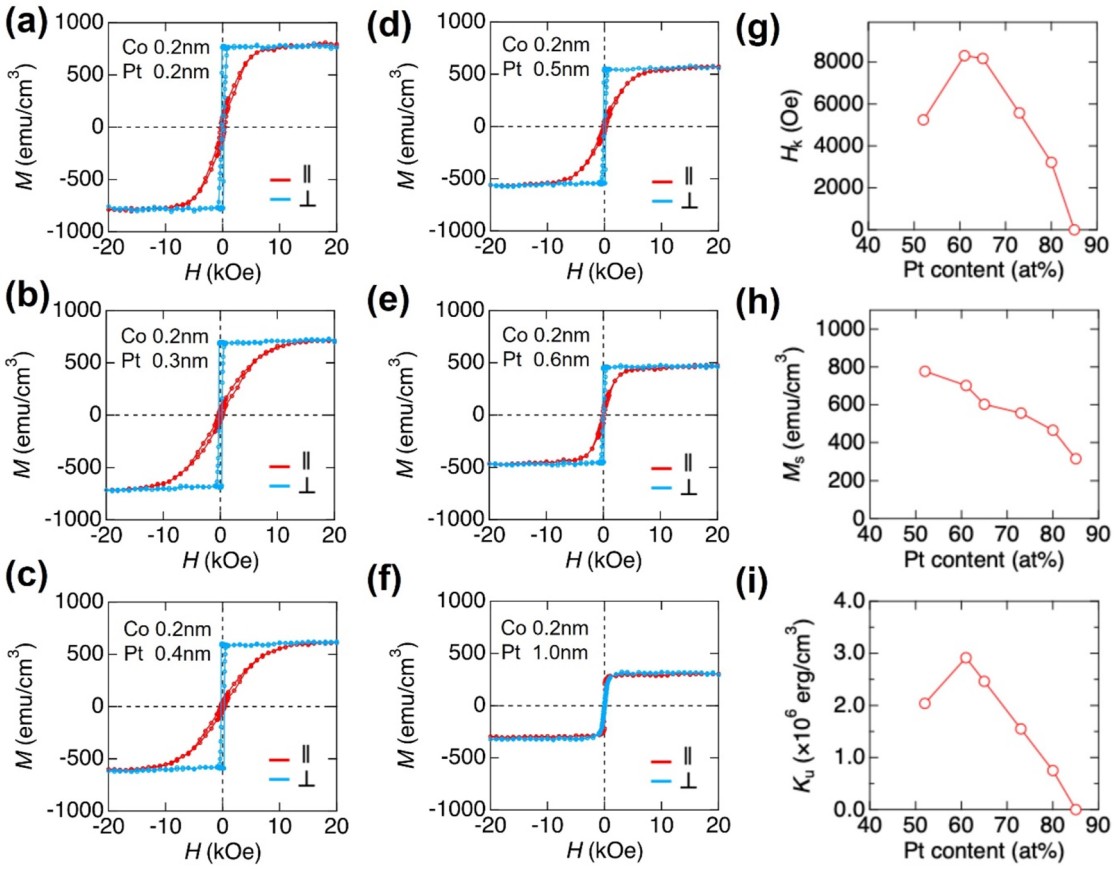

FIG. 3. (a)–(f) Magnetic hysteresis loops of substrate/Ru 40 nm/[Co 0.2 nm/Pt x nm]$_y$ multilayers (x is shown on the graphs). (g)–(i) Pt content dependence of (g) H_k, (h) M_s, and (i) K_u.

present study. This non-integer monolayer controlled structure can be explained by the long-range periodicity formed by layer-by-layer like growth, in which CoPt alloy monoatomic layers may be formed with changing the composition in a well-defined manner. Compared with the symmetric alternate layered structure in which the two components have similar thicknesses, the results here proved that even in an imbalanced layered structure with one material kept at a fixed thickness, the non-integer control of another material layer can also reproduce the peak splitting feature. The formation of a well-defined interface throughout the structure demonstrates the potential of non-integer monoatomic layer-by-layer growth using sputtering on a high-quality buffer layer and optimized deposition procedure, which is expressive for further development of spintronic devices, especially for the utilization of interfacial electronic states.[5,10]

The magnetic properties of Co/Pt multilayers are shown in Fig. 3. Figures 3(a)–3(f) illustrate the M–H loops for the sample stacks of substrate/Ru 40 nm/[Co 0.2 nm/Pt x nm]$_y$ multilayer/Ru 2 nm cap with the Pt thickness (x) listed on the graph. The corresponding Pt atomic composition ratios are evaluated from the experimentally obtained Co and Pt thicknesses and the bulk densities of Co and Pt. First, the Co layer thickness was determined to be 0.175 nm from the XRD and EDS results of multilayer period Λ = 0.432 nm and chemical composition $Co_{48}Pt_{52}$ (at. %), respectively, for the [Co 0.2 nm/Pt 0.2 nm] multilayer. Second, based on the excellent linearity of the Co/Pt multilayer period (see Fig. S1 of the supplementary material), the Pt layer thicknesses were determined by subtracting the Co layer thickness (0.175 nm) from each Λ. The results are listed in Table I. Note that the number densities of Co and Pt are almost unchanged for pure Co, pure Pt, ordered CoPt alloy, and disordered CoPt alloy, showing the validity of the use of the bulk densities. The magnetic measurement was conducted with VSM, and the magnetization was calculated from the magnetic moment obtained with the nominal thickness and the film area size. The PMA effect is observed for x varying from 0.2 to 0.6 nm, and all the out-of-plane hysteresis loops have sharp magnetization reversals with good squareness, together with the well-defined linearity of in-plane hysteresis. Only the [Co 0.2 nm/Pt 1.0 nm]$_8$ multilayer showed no PMA probably due to the large amount of Pt, as indicated by the distinct bulk Pt(111) peak in the XRD results.

The Pt content dependence of H_k, M_s, and K_u is shown in Figs. 3(g)–3(i), respectively. The maximum of K_u was shown up at 61% and then decreased with increasing the Pt content, which appears to be consistent with the previous study using a co-sputter method.[1] This result indicates that our multilayer deposition can sufficiently control the Co/Pt composition ratio through the non-integer monoatomic layer manner, comparable with the co-sputter method. A remarkable aspect of the maximum K_u is that the multilayered film does not show the $L1_1$ ordered peak but incommensurate split superlattice peaks. Meanwhile, the absolute value of K_u is 3 × 10^6 erg/cm^3, which is much smaller than that of the co-sputtered $L1_1$-like CoPt films. This may be explained by the long-range but partial ordering in the Co/Pt multilayer. M_s gradually decreases from 777 to 317 emu/cm^3 with an increase in the Pt composition from 52% to 85%. The coercivity varies between 150 and 300 Oe, following the trend of the composition dependence of K_u. Note that while the properties of Co/Pt multilayers are very sensitive to multiple parameters such as temperature,[1,11,12] deposition pressure,[13–15] the sputtering gas ambience,[13] and multilayer structure,[6,16–19] etc.,[20,21] the non-integer monolayer controlled Co/Pt multilayers may provide a comprehensive way to manipulate the magnetic properties by modulating the Co/Pt composition and the accuracy is comparable to the co-sputter method.

The cross-sectional HAADF-STEM images of the stack with a 0.2 nm thick Pt layer are shown in Figs. 4(a) and 4(b). From the fast Fourier transform (FFT)-filtered image, a perfect lattice matching with a misfit dislocation-free Ru/[Co/Pt] interface was observed, which follows our designed epitaxial relationship. In this HAADF-STEM image, the atoms such as Pt with higher atomic numbers produce brighter image contrast. In the two different squared regions of the Co/Pt multilayer, a weak but $L1_1$-like contrast can be observed, supporting the scenario of partial ordering discussed in the paragraph of magnetic properties. A corresponding atomic model is also illustrated for the Ru/[Co/Pt] stack in Fig. 4(c). From the EDS line profile [Fig. 4(d)], the atomic ratio of Co to Pt is estimated to be 48:52, which is consistent with the single superlattice peak of XRD, indicating a nearly perfect 50:50 composition. Nevertheless, there is no apparent delamination, and the $L1_1$-like structure can be observed in several limited areas, resulting in the feature of disordering in the Co/Pt film, which may be attributed to the low deposition pressure. Although the disordered structure suppressed a high K_u, a low-pressure deposition ambience constructed the high-quality flatness and crystallinity.

In this work, non-integer monoatomic layer-controlled epitaxial Co/Pt multilayer structures were obtained with clear incommensurate superlattice periodicity. The unique peak splitting behavior in the out-of-plane XRD results was analyzed with the systematic variation of the Pt content. It should be emphasized that the incommensurate Co/Pt superlattice structure survives down to an atomic scale like the [Co 0.2 nm/Pt 0.2 nm] multilayer formed by "sputtering." The magnetization measurement showed that a maximum of K_u of 3 × 10^6 erg/cm^3 was obtained for the multilayer with 61% Pt, which exhibits incommensurate superlattice reflection instead of the $L1_1$-ordered peak. In addition to the cross-sectional microstructural observation, the magnetic measurements suggest that the observed incommensurate superlattice periodicity is rather long-range but only due to incomplete compositional contrast of Co and Pt. This study demonstrates an important aspect of the superlattice structure in sputter-deposited Co/Pt multilayers.

TABLE I. Designed and experimentally determined structures for the Co/Pt multilayers. The atomic ratios are evaluated from the XRD and EDS analyses and the calculations with bulk densities for Co and Pt.

Designed structure (nm)	Experimentally determined structure (nm)	Atomic ratio
Co (0.2)/Pt (0.2)	Co (0.175)/Pt (0.257)	Co 48/Pt 52
Co (0.2)/Pt (0.3)	Co (0.175)/Pt (0.369)	Co 39/Pt 61
Co (0.2)/Pt (0.4)	Co (0.175)/Pt (0.438)	Co 35/Pt 65
Co (0.2)/Pt (0.5)	Co (0.175)/Pt (0.646)	Co 27/Pt 73
Co (0.2)/Pt (0.6)	Co (0.175)/Pt (0.762)	Co 20/Pt 80
Co (0.2)/Pt (1.0)	Co (0.175)/Pt (1.175)	Co 15/Pt 85

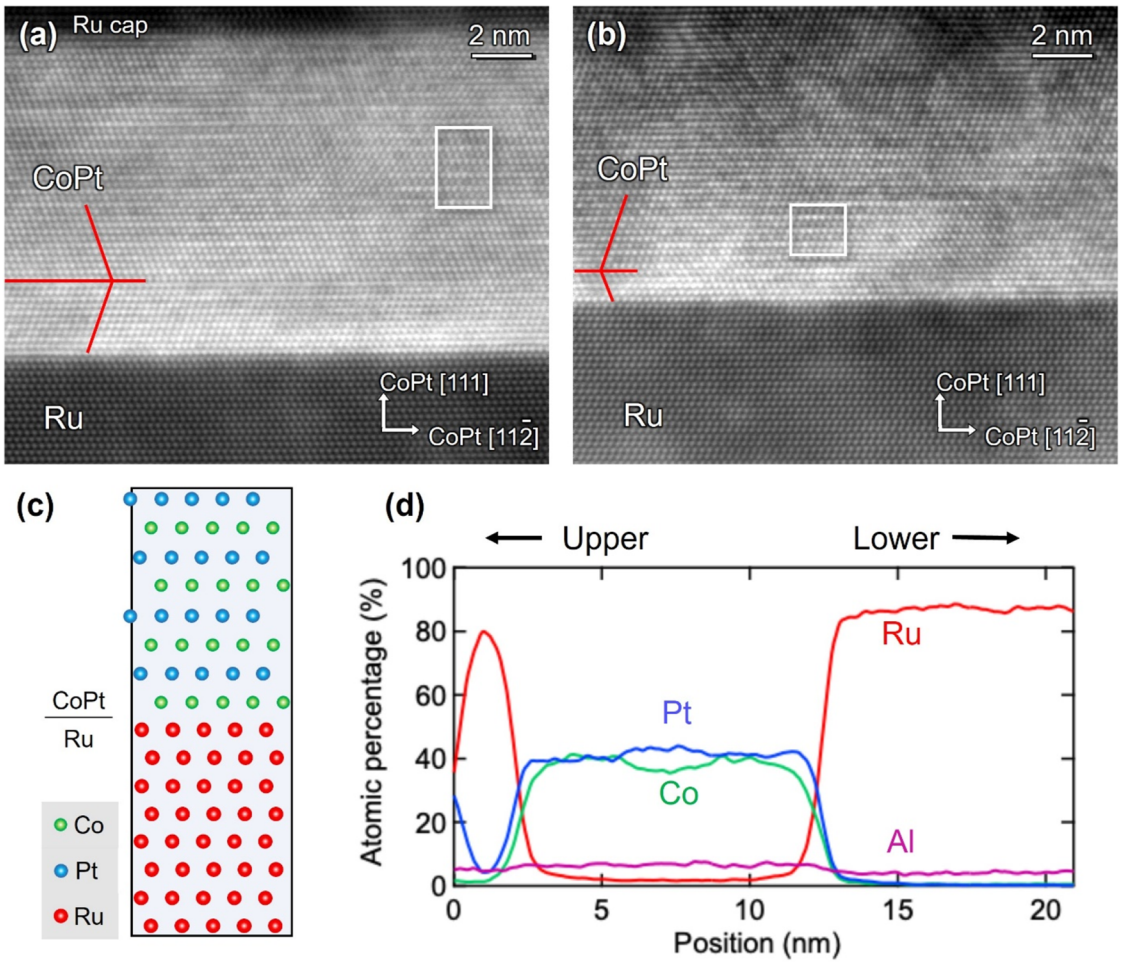

FIG. 4. (a) and (b) Cross-sectional HAADF-STEM images of two different areas for a Ru (40 nm)/[Co 0.2 nm/Pt 0.2 nm]$_{24}$/Ru 2 nm stack observed along $Al_2O_3[10\bar{1}0]$. (c) Illustration of an atomic model for the Ru/[Co/Pt] stack. (d) EDS elemental depth profiles of [Co 0.2 nm/Pt 0.2 nm]$_{24}$. The Co/Pt multilayer composition was evaluated to be $Co_{48}Pt_{52}$ from the profiles.

See the supplementary material for the linearity of the Co/Pt multilayer period.

ACKNOWLEDGMENTS

This work was partly supported by JST CREST (Grant No. JPMJCR19J4), JSPS KAKENHI under Grant Nos. 22H04966 and 24H00408, and Samsung Advanced Institute of Technology. J.S. acknowledges the National Institute for Materials Science for the provision of a NIMS Junior Research Assistantship.

AUTHOR DECLARATIONS

Conflict of Interest

The authors have no conflicts to disclose.

Author Contributions

Jieyuan Song: Data curation (equal); Formal analysis (equal); Writing – original draft (equal). **Thomas Scheike**: Data curation (supporting); Formal analysis (supporting); Writing – review & editing (equal). **Cong He**: Data curation (lead); Formal analysis (lead). **Zhenchao Wen**: Data curation (supporting); Formal analysis (supporting); Writing – review & editing (equal). **Tadakatsu Ohkubo**: Data curation (supporting); Formal analysis (supporting); Writing – review & editing (equal). **Kwangseok Kim**: Conceptualization (equal); Supervision (equal). **Hiroaki Sukegawa**: Conceptualization (equal); Data curation (supporting); Formal analysis (lead); Funding acquisition (equal); Supervision (equal); Writing – review & editing (equal). **Seiji Mitani**: Funding acquisition (equal); Supervision (equal); Writing – review & editing (equal).

DATA AVAILABILITY

The data that support the findings of this study are available within the article and from the corresponding authors upon reasonable request.

REFERENCES

[1]H. Sato, T. Shimatsu, Y. Okazaki, H. Muraoka, H. Aoi, S. Okamoto, and O. Kitakami, "Fabrication of $L1_1$ type Co-Pt ordered alloy films by sputter deposition," J. Appl. Phys. **103**, 07E114 (2008).

[2]K. Yakushiji, H. Kubota, A. Fukushima, and S. Yuasa, "Perpendicular magnetic tunnel junctions with strong antiferromagnetic interlayer exchange coupling at first oscillation peak," Appl. Phys. Express **8**, 083003 (2015).

[3]N. Tezuka, S. Oikawa, I. Abe, M. Matsuura, S. Sugimoto, K. Nishimura, and T. Seino, "Perpendicular magnetic tunnel junctions with low resistance-area product: High output voltage and bias dependence of magnetoresistance," IEEE Magn. Lett. **7**, 3104204 (2016).

[4]J.-Y. Choi, D. Lee, J.-U. Baek, and J.-G. Park, "Double MgO-based perpendicular magnetic-tunnel-junction spin-valve structure with a top $Co_2Fe_6B_2$ free layer using a single SyAF $[Co/Pt]_n$ layer," Sci. Rep. **8**, 2139 (2018).

[5]K. Masuda, H. Itoh, Y. Sonobe, H. Sukegawa, S. Mitani, and Y. Miura, "Interfacial giant tunnel magnetoresistance and bulk-induced large perpendicular magnetic anisotropy in (111)-oriented junctions with fcc ferromagnetic alloys: A first-principles study," Phys. Rev. B **103**, 064427 (2021).

[6]K. Yakushiji, T. Saruya, H. Kubota, A. Fukushima, T. Nagahama, S. Yuasa, and K. Ando, "Ultrathin Co/Pt and Co/Pd superlattice films for MgO-based perpendicular magnetic tunnel junctions," Appl. Phys. Lett. **97**, 232508 (2010).

[7]I. K. Schuller, M. Grimsditch, F. Chambers, G. Devane, H. Vanderstraeten, D. Neerinck, J.-P. Locquet, and Y. Bruynseraede, "Coherency of interfacial roughness in GaAs/AlAs superlattices," Phys. Rev. Lett. **65**, 1235 (1990).

[8]S. Mitani, K. Takanashi, Y. Shigemoto, and H. Fujimori, "Coherent layered structures in Fe/Au monatomic multilayers with addition of fractional atomic layers," Jpn. J. Appl. Phys. **36**, L1045 (1997).

[9]M. Ohtake, D. Suzuki, M. Futamoto, F. Kirino, and N. Inaba, "Preparation of $L1_1$-CoPt/MgO/$L1_1$-CoPt tri-layer film on Ru(0001) underlayer," AIP Adv. **6**, 056103 (2016).

[10]K. Masuda, H. Itoh, and Y. Miura, "Interface-driven giant tunnel magnetoresistance in (111)-oriented junctions," Phys. Rev. B **101**, 144404 (2020).

[11]A.-C. Sun, F.-T. Yuan, J.-H. Hsu, and H. Y. Lee, "Evolution of structure and magnetic properties of sputter-deposited CoPt thin films on MgO(111) substrates: Formation of the $L1_1$ phase," Scr. Mater. **61**, 713 (2009).

[12]M. Ohtake, S. Ouchi, F. Kirino, and M. Futamoto, "Structure and magnetic properties of CoPt, CoPd, FePt, and FePd alloy thin films formed on MgO(111) substrates," IEEE Trans. Magn. **48**, 3595 (2012).

[13]G. A. Bertero and R. Sinclair, "Structure-property correlations in Pt/Co multilayers for magneto-optic recording," J. Magn. Magn. Mater. **134**, 173 (1994).

[14]N. Honda, S. Hinata, and S. Saito, "Layer stacked Co/Pt films with high perpendicular anisotropy sputter deposited at room temperature," AIP Adv. **7**, 056518 (2017).

[15]K.-W. Park, Y.-W. Oh, D.-H. Kim, J.-Y. Kim, and B.-G. Park, "Effect of sputtering pressure on stacking fault density and perpendicular magnetic anisotropy of CoPt alloys," J. Phys. D: Appl. Phys. **49**, 345002 (2016).

[16]M. Ohtake, D. Suzuki, M. Futamoto, F. Kirino, and N. Inaba, "Effect of composition on the ordered phase formation in Co-Pt thin film deposited on MgO(111) single-crystal substrate," IEEE Trans. Magn. **50**, 2104004 (2014).

[17]T.-C. Yang, Y.-S. Chen, Y.-C. Ju, Y.-T. Lin, C.-F. Huang, H.-C. Lu, S.-F. Wang, P. Sharma, and A.-C. Sun, "Effects of thickness ratio of Co to Pt layer on magnetic properties and microstructure of $[Co/Pt]_n$ multilayer films," IEEE Trans. Magn. **51**, 2301904 (2015).

[18]G. C. Hermosa and A.-C. Sun, "Sputtered high perpendicular magnetic anisotropy CoPt thin film on flexible substrate at low temperature," AIP Adv. **10**, 015132 (2020).

[19]C.-F. Huang, A.-C. Sun, H.-Y. Wu, F.-T. Yuan, J.-H. Hsu, S.-N. Hsiao, H.-Y. Lee, H.-C. Lu, S.-F. Wang, and P. Sharma, "Fabrication of $L1_1$ phase CoPt film on glass substrate with [Co/Pt] multilayer structure," IEEE Trans. Magn. **50**, 3201804 (2014).

[20]M. Bersweiler, K. Dumesnil, D. Lacour, and M. Hehn, "Impact of buffer layer and Pt thickness on the interface structure and magnetic properties in (Co/Pt) multilayers," J. Phys. Condens. Matter **28**, 336005 (2016).

[21]S. T. Lim, M. Tran, J. W. Chenchen, J. F. Ying, and G. Han, "Effect of different seed layers with varying Co and Pt thicknesses on the magnetic properties of Co/Pt multilayers," J. Appl. Phys. **117**, 17A731 (2015).